

Eclipses Observed by *Large Yield RAdiometer* (LYRA) – A Sensitive Tool to Test Models for the Solar Irradiance

A.I. Shapiro · W. Schmutz · M. Dominique ·
A.V. Shapiro

Received: 16 August 2011 / Accepted: 1 July 2012 / Published online: 31 July 2012
© Springer Science+Business Media B.V. 2012

Abstract We analyze the light curves of the recent solar eclipses measured by the Herzberg channel (200–220 nm) of the *Large Yield RAdiometer* (LYRA) onboard *Project for On-Board Autonomy* (PROBA2). The measurements allow us to accurately retrieve the center-to-limb variations (CLV) of the solar brightness. The formation height of the radiation depends on the observing angle, so the examination of the CLV provide information about a broad range of heights in the solar atmosphere. We employ the 1D NLTE radiative transfer *COde for Solar Irradiance* (COSI) to model the measured light curves and corresponding CLV dependencies. The modeling is used to test and constrain the existing 1D models of the solar atmosphere, *e.g.* the temperature structure of the photosphere and the treatment of the pseudo-continuum opacities in the Herzberg continuum range. We show that COSI can accurately reproduce not only the irradiance from the entire solar disk, but also the measured CLV. Hence it can be used as a reliable tool for modeling the variability of the spectral solar irradiance.

PROBA2 – First Two Years of Solar Observation

Guest Editors: David Berghmans, Anik De Groof, Marie Dominique, and Jean-François Hochedez

A.I. Shapiro (✉) · W. Schmutz · A.V. Shapiro

Physikalisch-Meteorologisches Observatorium Davos, World Radiation Center, 7260 Davos Dorf,
Switzerland

e-mail: alexander.shapiro@pmodwrc.ch

W. Schmutz

e-mail: werner.schmutz@pmodwrc.ch

A.V. Shapiro

e-mail: anna.shapiro@pmodwrc.ch

M. Dominique

Royal Observatory of Belgium, Ringlaan 3, 1180 Brussel, Belgium

e-mail: Marie.Dominique@oma.be

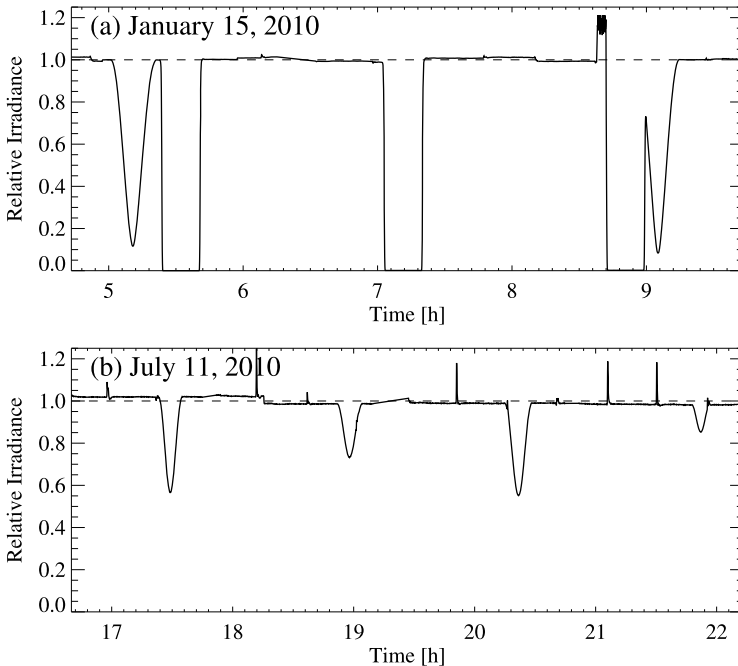


Figure 1 Relative variations of the irradiance as measured by the Herzberg channel of LYRA. The intervals of zero intensity occur during occultations when PROBA2 passes throughout the Earth shadow in the winter season. The panels show two eclipses separated by the three occultations on 15 January 2010 (a) and four eclipses on 11 July 2010 (b). The periodic, abrupt changes of the irradiance level are due to the spacecraft maneuvers.

1. Introduction

The variability of the solar irradiance may have a direct impact on climate (Haigh, 2007; Gray *et al.*, 2010). Although the measurements and modeling of the solar irradiance were under close attention during the last decade, the complete picture of the solar variability is still far from being clear (Harder *et al.*, 2009; Haigh *et al.*, 2010). Therefore the launch of every new space mission devoted to the measurements of the solar irradiance is able to provide a crucial piece of complementary information, as well as to nourish theoretical models.

In this article we analyze the first measurements of *Large Yield Radiometer* (LYRA: Hochedez *et al.*, 2006; Benmoussa *et al.*, 2009) onboard the *Project for OnBoard Autonomy* (PROBA2) satellite launched on 2 November 2009. LYRA has observed several solar eclipses (see Figure 1).

During an eclipse, the Moon consecutively covers different parts of the solar disk. The light curve of the eclipse depends on the CLV of the solar brightness and on the geometry of the eclipse (the angular radii of the Sun and the Moon as well as the minimum distance between their centers which is reached during the maximum phase of the eclipse). If the geometry of the eclipse is known and the distribution of solar brightness has radial symmetry, then the light curve of the eclipse can be used to retrieve the CLV of the solar brightness. Let us note that the assumption of radial symmetry is well-justified for the 15 January 2010 eclipse as the solar-activity level was very low (according to the USAF/NOAA data the total

sunspot area was about 0.025 % of the full solar disk). The CLV of the solar brightness provides valuable information about the solar atmosphere (Allende Prieto, Asplund, and Fabiani Bendicho, 2004; Koesterke, Allende Prieto, and Lambert, 2008) and determines the irradiance variations on the time-scale of solar rotation (Fligge, Solanki, and Unruh, 2000). Additionally the changes of the spectral solar irradiance during eclipses are important for studying the Earth's atmospheric response (Kishore Kumar, Subrahmanyam, and John, 2011; Sumod *et al.*, 2011).

Shapiro *et al.*, 2010 showed that the 1D NLTE radiative transfer *COde for Solar Irradiance* (COSI: Haberreiter, Schmutz, and Hubeny, 2008) allows one to calculate the solar spectrum (125 nm – 1 μ m) from the entire solar disk with high accuracy. In this article we use COSI to calculate the CLV of the solar brightness and compare it with ones deduced from the eclipse light curves as observed by LYRA. We show that the measured CLV provides an important constraint on the UV opacities and the temperature structure of the solar atmosphere. We come up with a model that allows us to accurately reproduce the measurements.

We restrict ourselves to the modeling of the eclipse profiles and CLV in the Herzberg channel of LYRA. The solar irradiance in the Herzberg continuum range (200–220 nm) is of special importance for climate modeling as it directly affects the ozone concentration and stratospheric temperature (Brasseur *et al.*, 1987; Rozanov *et al.*, 2006; Shapiro *et al.*, 2011c). The proper modeling of the formation of this radiation in the solar atmosphere is fundamental for variability modeling and for irradiance reconstruction in the past (Krivova, Solanki, and Unruh, 2011; Vieira *et al.*, 2011; Shapiro *et al.*, 2011a).

We are aware that the 1D models do not necessarily reflect the average physical properties of the inhomogeneous solar atmosphere (Uitenbroek and Criscuoli, 2011). Thus the main goal of this article is not to learn new facts about the dynamic 3D solar atmosphere but rather to develop a reliable semi-empirical tool for modeling the solar-irradiance variability.

In Section 2 we deduce the empirical CLV from the LYRA observations of the 15 January 2010 eclipse. In Section 3 we compare these CLVs with ones calculated by COSI and discuss the constraint on the temperature structure of the solar atmosphere (Section 3.2) and UV opacities (Section 3.3). The main results are summarized in Section 4.

2. Empirical Center-to-Limb Variations as Deduced from the LYRA Observations

PROBA2 has a dawn–dusk heliosynchronous orbit, with an altitude of 720 km on average, which allows quasi-permanent observations of the Sun. The spacecraft completes a full orbit in about 100 minutes. In the case of a solar eclipse, it is therefore not unusual that it crosses the eclipse zone more than once. LYRA data in the Herzberg channel are acquired, for all three units, by PIN detectors made of diamond. Such detectors have proven to be very stable with respect to temperature variations (Benmoussa *et al.*, 2004). There are no dioptric/catadioptric optics ahead of LYRA detectors, so no stray light is expected. The nominal cadence of acquisition is 20 Hz. A more detailed discussion of the in-flight performance of LYRA is given by Dominique *et al.* (2012).

The first light curve of an eclipse was obtained by LYRA on 15 January 2010. The eclipse was preceded by LYRA first light on 6 January 2010 and was the longest annular solar eclipse of the millennium. It was observed on the ground from Africa and Asia and was seen as partial from PROBA2. The eclipse lasted more than six hours, so PROBA2 passed through the Moon's umbra three times. However the intermediate transit could not be observed due to the simultaneous occultation (it was eclipsed by the Earth).

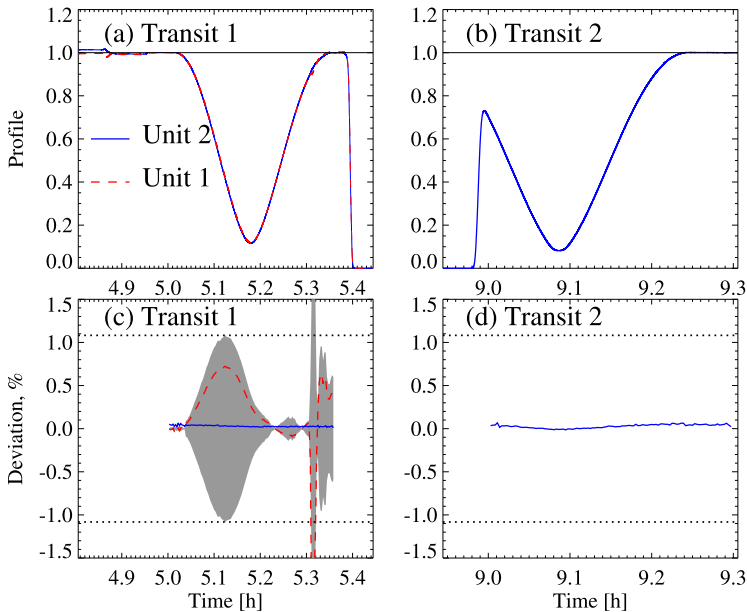


Figure 2 The profiles of the 05:00 (a) and 09:00 (b) transits retrieved from the level-1 data as well as the deviations between these profiles and the profile retrieved from the level-2 data of unit 2 (c, d). The shaded area on panel (c) indicates the estimated error range. The dotted lines correspond to the widest part of the error range in the time interval between 5 and 5.3 hours (*i.e.* excluding the problematic feature after 5.3 hours).

The raw (level 1) data collected by the Herzberg channel of LYRA during this eclipse are presented in panels a and b of Figure 2. The data were corrected for the dark current, which is present in the original data. The 05:00 UTC transit of the 15 January 2010 eclipse (hereafter first transit) was simultaneously observed by the LYRA units 1 and 2 (the back-up and standard acquisition units, accordingly), while the 09:00 UTC transit (hereafter second transit) only by the unit 2. The drops of the irradiance after the first and before the second transits correspond to the occultations (see panel a of Figure 1).

The level 1 data are uncalibrated. The calibrated (level 2) data are also available for the community. For the analysis presented below, we will therefore use the profiles retrieved from the level-2 data. These data are corrected for the temperature effects, degradation, and the dark current. Let us note that level-2 data always refer to the unit-2 measurements, while the measurements from the back-up units 1 and 3 are normally used for calibration and currently only available in their uncalibrated version (see the detailed description of the available data by Dominique *et al.*, 2012). Originally the level-2 data were corrected for the degradation by adding a time-dependent offset (to allow a better analysis of the solar flares). The offset shifts the zero-level of the irradiance and leads to the erroneous profiles of the eclipses and solar variability (Shapiro *et al.*, 2011d). Therefore, for our analysis, the offset was removed from the level-2 data.

The blue curves on panels c and d of Figure 2 represent the deviations between the level-1 and level-2 data. The zero-level of both datasets was corrected as discussed above. One can see that the level-2 data are almost identical to the original measurements of the standard acquisition unit 2. This confirms that the temperature correction for the diamond detectors is very small. From now on we will not distinguish between the level-1 and level-2 data of

unit 2. On the contrary there is a significant deviation between the data collected by unit 1 and unit 2 during the first transit. Both units were carefully calibrated in the ground facilities, so their different responses are connected with the degradation which affects the sensitivities of the units. The standard acquisition unit 2 was opened almost constantly, while the back-up units 1 and 3 were opened only occasionally. As a result by 15 January 2010 unit 2 had degraded approximately by 15 % while unit 1 did not yet show any noticeable degradation. The differential behavior of the units allows us to estimate the error range of the measured profiles. We defined the uncertainty as twice the difference between the profiles as observed by unit 2 and unit 1 (see Figure 2). This approach does not include any systematic deviations, common to both units but it measures the degradation due to space exposure. The arbitrary character of this estimate does not affect the results presented below. The second transit was only observed by unit 2, so for its analysis we will use the error range defined from the first transit.

The profile of the irradiance variation during the eclipse depends on the CLV of the solar brightness. For example a strong decrease of the brightness towards the solar limb would lead to a smaller residual irradiance during the maximal phase of the eclipse and accordingly to a deeper eclipse profile. Thus, the observed profiles allow us to determine the CLV. For simplicity we adopted a widely used polynomial parametrization of the CLV (Neckel and Labs, 1994; Neckel, 2005):

$$\frac{I(\mu)}{I_{\text{center}}} = \sum_i A_i \mu^i, \quad (1)$$

where I_{center} is the disk-center intensity, μ is the cosine of the heliocentric angle, and A_i are free parameters. The solar disk was divided into the thirteen supposedly uniform concentric rings and the brightness of each ring was calculated with the help of Equation (1) using the μ value of the ring's mean circle. We checked that such division of the solar disk allows us to calculate the irradiance profiles with accuracy better than 0.02 % and thus is sufficient for our purposes. Simple geometrical calculations allow us to obtain the profile of the eclipse for each set of the coefficients, assuming that the time dependencies of the angular distance between the Sun and the Moon as well as of their angular sizes are known.

For the both transits of the 15 January 2010 eclipse we searched for the set of the coefficients A_i that lead to the best agreement with the observed profiles and minimized the error defined as

$$\mathcal{E} = \sum_i (\mathcal{P}_{\text{obs}}^i - \mathcal{P}_{\text{emp}}^i)^2,$$

where \mathcal{P}_{obs} is the observed profile and \mathcal{P}_{emp} is the empirical profile calculated from Equation (1). For the first and second transits the summation was done over the time intervals between 5 and 5.3 hours and between 9 and 9.25 hours respectively.

The least-square minimization was performed applying the additional condition of the monotonic CLV. The CLV profiles were calculated using the second-degree polynomial. The employment of the higher-degree polynomial (up to sixth degree) had no visible effect. The CLV depends on the wavelength (Neckel, 1996; Hestroffer and Magnan, 1998). Thus, the coefficients determined by the minimization procedure correspond to the CLV of the solar intensity convolved with the profile of the LYRA Herzberg channel. The latter is a combined profile of the detector and filter.

The resulting empirical CLV dependencies are presented in Figure 3. The CLV dependency for the first transit is normalized to unity at the disk center, while all other CLV dependencies are normalized to give the same integral flux from the entire disk. The error

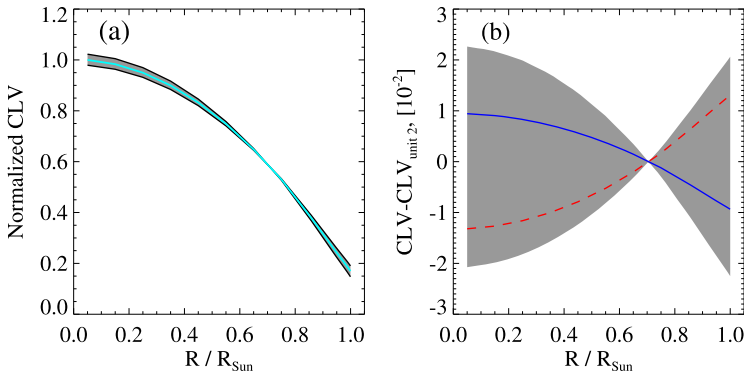


Figure 3 (a) Empirical CLV deduced from the profile of the first transit as observed by unit 2 (cyan curve); (b) the deviations between the CLV plotted on panel (a) and the CLV deduced from the profile of the first transit as observed by unit 1 (red dashed curve) and CLV deduced from the profile of the second transit as observed by unit 2 (blue curve). The empirical CLV deduced from the two extreme profiles corresponding to the edges of the error range in Figure 2 delimit the CLV error range (the shaded area).

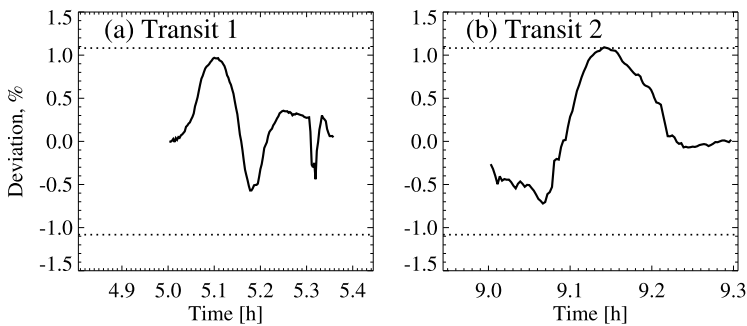


Figure 4 The deviations between the profiles as measured by unit 2 and as calculated with the empirical CLV. The error bars (dotted lines) are the same as in Figure 2.

range of the CLV was estimated performing the minimization procedure to the two maximal error profiles of the first transit. So the shaded area in Figure 3 is constrained by the two CLV dependencies which correspond to the edges of the shaded area in Figure 2.

The deviations between the profiles as measured by LYRA and calculated with the empirical CLV are shown in Figure 4. The deviations can be attributed to the limited accuracy of the measurements (note that they are within the estimated error bars) and to the violation of the assumed radial symmetry of the solar brightness. One of the sources of the asymmetry of the solar brightness is the inhomogeneous structure of the quiet Sun, which consists of several brightness components (Fontenla *et al.*, 1999). The small amplitude of the deviations supports the analysis presented below.

3. Comparison with Modeling

To calculate the theoretical CLV, we employed the 1D NLTE radiative transfer code COSI developed by Hubeny (1981), Hamann and Schmutz (1987), Schmutz, Hamann, and Wes-

solowski (1989), Haberreiter, Schmutz, and Hubeny (2008), and Shapiro *et al.* (2010). COSI simultaneously solves the statistical-equilibrium and radiative-transfer equations in the spherically symmetrical geometry. The temperature and density structures of the different components of the solar atmosphere were taken from Fontenla *et al.* (1999), while the electron density and all level populations were self-consistently calculated in NLTE.

3.1. Solar Irradiance in the Herzberg Continuum Range

The proper calculation of the radiative transfer in the Herzberg continuum region is complicated by two factors. Firstly, the continuum opacity in this region is strongly affected by NLTE overionization (Shchukina and Trujillo Bueno, 2001; Short and Hauschildt, 2005), so proper NLTE calculations are necessary. Secondly, the immense number of weak, mostly spectrally unresolved, lines form the so-called UV-line haze in this region. The creation of the correct line list, which would include all possible spectral lines, is a task of a tremendous difficulty. Although considerable progress was achieved during the last few decades, only 1 % of the UV lines are measured in the laboratory, while all remaining lines are only predicted theoretically (Kurucz, 2005). As a consequence the existing line lists are not complete and underestimate the opacity in the UV spectral region (Busá *et al.*, 2001; Haberreiter, Schmutz, and Hubeny, 2008; Short and Hauschildt, 2009).

To account for the missing opacity, Shapiro *et al.* (2010) multiplied the continuum opacity coefficient by the wavelength-dependent coefficient:

$$k'_c(\lambda) = k_c(\lambda) f_c(\lambda). \quad (2)$$

The multiplicative coefficient that we employed is a step function of the wavelength with a step size of 1 nm. It was empirically determined so that the UV irradiance calculated by COSI equals the irradiance as measured by *SOLar-STellar Irradiance Comparison Experiment* (SOLSTICE: McClintock, Snow, and Woods, 2005) onboard the *SORCE* satellite (Rottman, 2005) during the 2008 solar minimum. The additional opacity that is necessary to reproduce the *SORCE/SOLSTICE* irradiance does not exceed a few percent of the total opacity included in COSI. It is only necessary in the 160–320 nm spectral region. Shortward of 160 nm, the total opacity is mainly dominated by the photo-ionization continuum opacity, while longward of 320 nm the existing line lists are accurate enough to reproduce the irradiance with better than 5 % accuracy (and with better than 2 % accuracy longward of 400 nm).

As during the solar minimum the solar irradiance (except the extreme UV) is dominated by the quiet Sun, the solar atmosphere Model C (average supergranule cell interior model) from Fontenla *et al.* (1999) was used for the calculations. Let us however note that it would be possible to be in agreement with the *SORCE/SOLSTICE* measurements while using another temperature profile by adjusting additional opacities. Thus the *SORCE/SOLSTICE* measurements alone do not allow us to constrain the temperature structure of the solar atmosphere. In Section 3.2 we show that although simultaneous adjustment of the temperature structure and additional opacities does not affect the irradiance from the entire solar disk, it significantly changes the CLV. The comparison with the measured CLV allows us to choose the most suitable for the CLV calculations model.

Shapiro *et al.* (2010) assumed that the coefficient of the additional opacity does not depend on height in the solar atmosphere. This implies that it does not have any dominant source as the concentration of any particular ion or molecule is height dependent. In Section 3.3 we show that the CLV provide an important complementary information which allow us to reevaluate this assumption and help to understand the nature of the additional opacity.

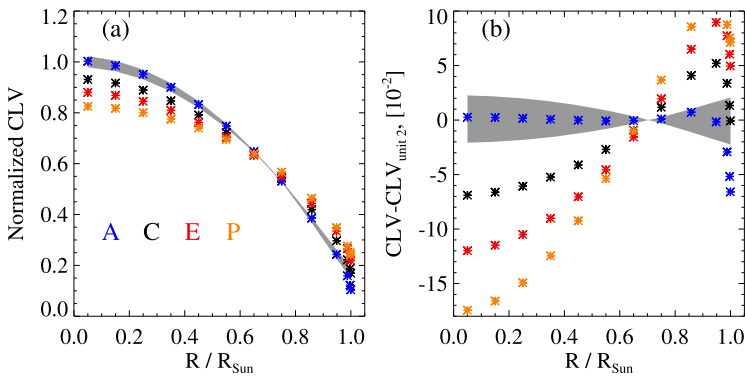


Figure 5 The CLV dependencies calculated for the faint supergranule cell interior (A), average supergranule cell interior (C), quiet network (E), and plage (P). The shaded area indicate the error range of the empirical CLV.

3.2. Test of the Temperature Structure

To test the sensitivity of the CLV to the change of the temperature structure, we performed the calculations employing the models for several different components of the solar atmosphere: Model A (faint supergranule-cell interior), Model C (average supergranule-cell interior), Model E (quiet network), and Model P (plage). The temperature and density structures were taken from Fontenla *et al.* (1999). Models A and E correspond to the cold and warm components of the quiet Sun, while Model C represents the spatially averaged quiet Sun. Shapiro *et al.* (2010) showed that the calculations with the latter model can reproduce spectral irradiance measured by SOLSTICE (up to 320 nm) and *Solar Irradiance Monitor* (SIM; Harder *et al.*, 2005) (from 320 nm onward) onboard the *SORCE* satellite during the 2008 solar minimum, as well as *SOLAR SPECTral Irradiance Measurements* (SOLSPEC; Thuillier *et al.*, 2004) during the *ATLAS 3* mission in 1994 with high accuracy. They used Model C to calculate the $f_c(\lambda)$ factor (see Equation (2)) for the additional opacities in the 160–320 nm spectral range.

The same procedure of the $f_c(\lambda)$ factor fitting was performed for Models A and E. Model A is colder than Model C so it yields smaller UV irradiance. Thus a smaller additional opacity is necessary to reproduce the *SORCE/SOLSTICE* measurements in the 160–320 nm spectral region. Accordingly the use of Model E leads to a larger additional opacity. Model P yields such a high irradiance that it is not possible to reach the *SORCE/SOLSTICE* level by increasing the continuum opacity. Thus we did not recalculate the $f_c(\lambda)$ factor for Model P and left it the same as for Model C.

In Figure 5 we present the calculated CLV for each of these models. The radiation which comes from the regions close to the solar limb is formed in higher and colder regions of the solar atmosphere than the radiation coming from the disk center. Hence the solar brightness is decreasing towards the limb. One can see that the colder the model, the steeper CLV it yields. This can be partly explained by the fact that the sensitivity of the Planck function to the temperature change is a decreasing function of the temperature. Thus the same change of temperature results in a larger alteration of the Planck function and accordingly larger change of the emergent irradiance for the colder models. The complete picture depends on the temperature and density structure as well as on the opacity in each of the solar atmosphere components. It is further complicated by NLTE effects that causes deviations of the source function from the Planck function.

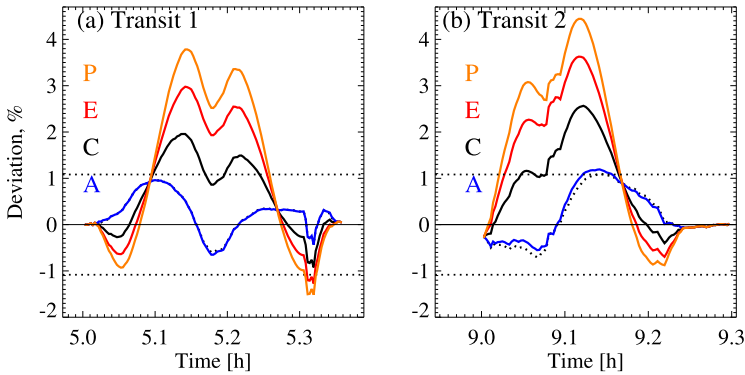


Figure 6 The deviations between the profiles as measured by unit 2 and as calculated for the solar atmosphere Models A, C, E, and P. The error bars (dotted lines) are the same as in Figure 2. The dotted curve corresponds to the profile calculated with the empirical CLV.

Although, due to the readjustment of the additional opacity, the calculations with Models A and E yield the same UV irradiance as the calculation with Model C, the corresponding CLV dependencies are remarkably different. All differences between the theoretical and empirical CLVs have a sudden drop at $R/R_{\text{Sun}} \approx 0.99$ (see Figure 5). The rings that correspond to these points (see Section 2) have very small relative area, so the eclipse profiles are basically insensitive to the change of their brightness. Thus the reliability of the empirical CLV for these points is very low.

Interestingly, the calculations with Model C underestimate the CLV and are outside of the estimated errors. One of the possible reasons for this could be the erroneous assumption of the depth independency of the additional opacity coefficient (see Equation (2)). This possibility will be discussed in Section 3.3. On the other hand, it is known that 1D models can underestimate the anisotropy of the radiation field (Shapiro *et al.*, 2011b; Kleint *et al.*, 2011) and the CLV of the solar brightness (Koesterke, Allende Prieto, and Lambert, 2008; Uitenbroek and Criscuoli, 2011). Hence the reported disagreement could be a signature of the general problems that are inherent to 1D modeling.

The warmer Models E and P yield even weaker CLV than Model C. At the same time the colder Model A yields a CLV that is in a good agreement with the empirical ones.

The corresponding deviations between the calculated and measured profiles are shown in Figure 6. The structure common to both transits represents properties of the models, while individual structure is due to the limited accuracy of the measurements and violation of the radial symmetry of the solar brightness. We can define the discrepancy between the profiles \mathcal{P}_1^i and \mathcal{P}_2^i as

$$\Delta_{1,2} = 10^{-4} \sqrt{\left(\sum_{i=1}^N (\mathcal{P}_1^i - \mathcal{P}_2^i)^2 / N \right)}, \tag{3}$$

where N is number of the time points in the profiles and the scaling factor 10^{-4} is introduced for convenience.

In Table 1 we present the discrepancies between the theoretical, measured, and empirical (calculated with the empirical CLV, see Section 2) profiles. One can see that the calculations with Model A are in good agreement with the measurements and are very close to the

Table 1 Theoretical profiles vs. observed and empirical (calculated with the empirical CLV) profiles. The numbers are discrepancies calculated with the help of Equation (3). The minimum values of the discrepancy are boldfaced.

	Passage 1		Passage 2	
	Observed	Empirical	Observed	Empirical
A	49.9	3.3	65.0	9.9
C	105.8	92.5	130.1	113.0
E	168.7	160.4	197.3	186.5
P	216.3	209.2	245.2	236.3

empirical profile. Let us however note that Model A is not able to properly reproduce the visible and near-infrared irradiance as well as the main molecular bands (*e.g.* CH *G-band* and CN *violet system*) in the solar spectrum. The calculations with Models E and P result in too weak CLV and consequently in too high residual irradiance during the maximal phase of the eclipse. Although the calculations with Model C are outside of the estimated error range, the resulting profiles are reasonably close to the observations (*e.g.* they will be hardly distinguishable from the measured ones on the scale of Figure 1). Thus Model C can still be used in the calculations when high accuracy is not necessary.

3.3. Adjustments of the Additional Opacities

The introduction of the additional opacity described in Section 3.1 changes the formation heights of the UV radiation and thus affects the CLV. All calculations presented in Section 3.2 were performed assuming depth-independent coefficient f_c in Equation (2). At the same time if the additional opacity arises from the unaccounted for lines of some particular atom or molecule X then it should be scaled with the relative concentration of X . Then the coefficient f_c becomes height dependent:

$$f_c(\lambda, h) = 1 + \mathcal{F}_c(\lambda) \frac{n_X(h)/n_{\text{total}}(h)}{(n_X(h)/n_{\text{total}}(h))_{\text{max}}}, \quad (4)$$

where h is the height in the solar atmosphere, and n_{total} and n_X are the total and species X concentrations respectively. $\mathcal{F}_c(\lambda)$ is a step function, which can be determined empirically in the same way as the f_c factor was determined by Shapiro *et al.* (2010). The height dependency of the additional opacity is introduced by the fraction in the right side of Equation (4). The latter is the relative concentration of the species X , normalized for convenience to unity.

To better understand the possible origin of the additional opacity, we scaled it with the relative concentrations of CN and CO molecules and Fe I ion. In each case we empirically determined the $\mathcal{F}_c(\lambda)$ factor to reproduce the SORCE/SOLSTICE UV measurements. In Figure 7(a) we show the dependency of the fraction from Equation (4) on height. The CN and CO molecules are mainly present in the narrow photospheric layer. As the CO molecule has larger dissociation potential than CN (11.1 eV against 7.76 eV) it is more sensitive to the temperature change (Berdyugina, Solanki, and Frutiger, 2003) and the maximum of the CO relative concentration is very close to the temperature minimum. The maximum of the CN relative concentration is slightly shifted towards the lower levels of the photosphere where the effect of the density increase overcompensate for the temperature increase. Iron is mostly ionized throughout the solar atmosphere. Similarly to the molecular case, the neutral-iron concentration has a peak slightly below the temperature minimum. At the same time it does not drop so abruptly in the lower level of the solar photosphere and starts to increase in the chromosphere due to the strong density decrease.

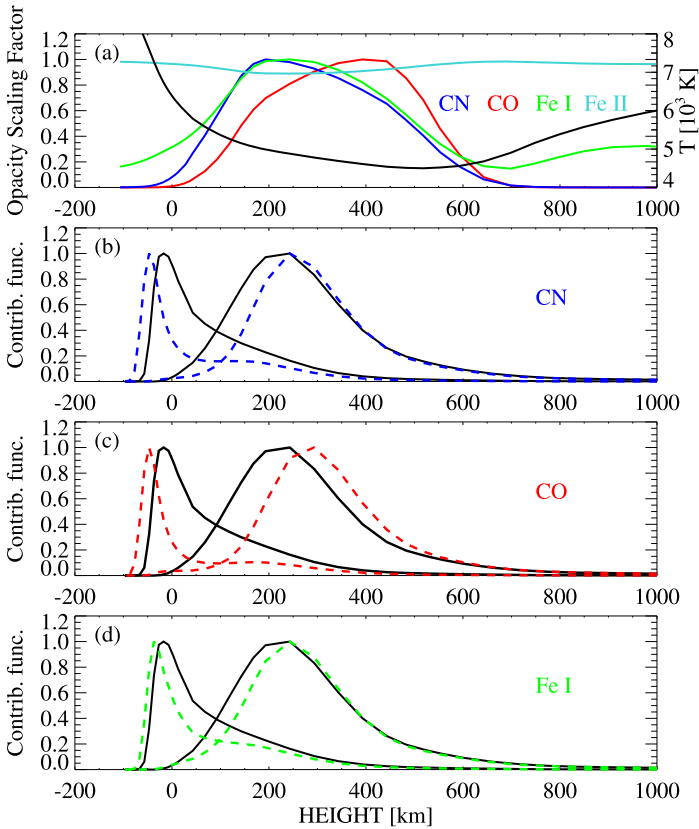


Figure 7 Opacity scaling factor (the fraction in the right side of Equation (4)) and temperature (black curve) as a function of height (a) as well as the contribution functions near the limb ($R/R_{\text{Sun}} = 0.95$) and disk center intensities. The contribution functions are shown for the case of height-independent additional opacity (black curves in (b), (c), and (d)) and additional opacity scaled with the CN (b), CO (c), and Fe I (d) relative concentrations. The zero-point of the height scale is defined as the layer at which the continuum optical depth at 500 nm is equal to one.

On the three lower panels of Figure 7 we show the contribution functions for the intensities in the Herzberg continuum range. They were obtained by convolving the individual contribution functions (Gray, 1992, p. 151) for every frequency with the combined profile of the detector and filter in the Herzberg channel. Thus the plotted contribution functions sample the regions where the irradiance measured by the Herzberg channel of LYRA is formed. The scaling of the additional opacity with the Fe I or molecular concentrations alters the optical depth scale and simultaneously shifts the limb and disk-center contribution functions to the higher and lower levels of the solar atmosphere respectively. This increases the distance between the peaks of the limb and disk center contribution functions, which results in the stronger CLV. The effect is most prominent for the scaling with the CO relative concentration (due to the strong shift of the limb contribution function) and least prominent for the Fe I case (due to a small effect on the disk-center contribution function).

The above discussion is confirmed by Figures 8 and 9 where the CLV dependencies and the eclipse profiles for the different cases of the additional opacity scaling are presented. One can see that the scaling of the additional opacity makes the CLV stronger.

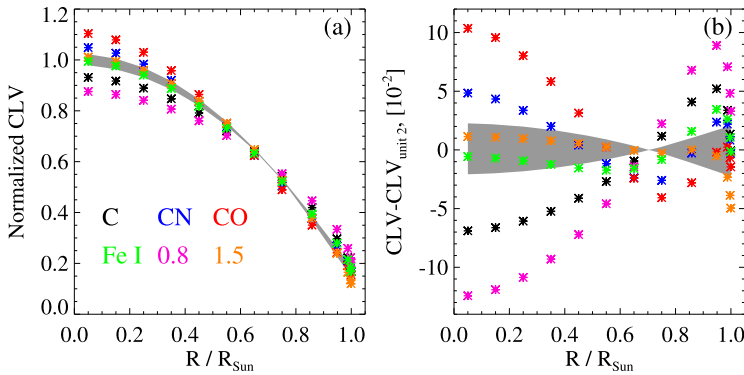


Figure 8 The CLV dependencies calculated for different modes of calculations with Model C. The “CN”, “CO”, and “Fe I” points were calculated scaling the additional opacity with the relative concentration of the corresponding species. The “0.8” and “1.5” points were calculated adjusting the additional opacity so that COSI yields 80 % and 150 % of the UV irradiance measured by the SORCE/SOLSTICE. The “C” points correspond to the standard calculations using Model C (*i.e.* with height independent additional opacities adjusted to reproduce the SORCE/SOLSTICE UV measurements). The shaded area indicates the error range of the empirical CLV.

The scaling with the CO relative concentration results in too strong a CLV and accordingly too small a residual irradiance during the maximal phase of the eclipse. At the same time, the scaling with the Fe I or CN relative concentrations moves the CLV dependencies and irradiance profiles very close to the observed ones and hence can solve the problem addressed in the end of Section 3.2. Let us note that, as opposed to the calculations with Model A, these calculations can also properly reproduce all main features in the solar spectrum.

While the relative variations of the irradiance can be measured by LYRA with a very high precision, the absolute calibration of the LYRA radiometers is very tricky and renders the determination of the absolute level of the irradiance almost impossible without the use of an external reference. The additional opacities in COSI were adjusted to reproduce the irradiance as measured by SORCE/SOLSTICE. If the solar UV irradiance were different from that measured by SORCE/SOLSTICE, then a different additional opacity would be necessary to reproduce it. The readjustment of the additional opacities will affect not only the absolute level of the measured irradiance but also the CLV. Thus the CLV deduced from the eclipse analysis can be used to indirectly test the SORCE/SOLSTICE measurements. With this goal we made two experiments readjusting the additional opacity so that COSI yields 80 % and 150 % of the SORCE/SOLSTICE irradiance (the same scaling factor was applied for all wavelengths in the 160–320 nm interval). In these experiments we followed the approach of Shapiro *et al.* (2010) and assumed that the f_c factor from Equation (2) is independent of height.

The corresponding CLV are given on Figure 8, while the eclipse profiles are plotted on the bottom panels of Figure 9. One can see that the increase of the absolute level of the irradiance leads to a stronger CLV and good agreement with the measurements. Let us note that due to the problem of the standard modeling discussed in Section 3.2 this should be considered not as a contradiction to the SORCE/SOLSTICE measurements but rather as a consequence of too weak a CLV yielded by the calculations with Model C and a depth-independent coefficient f_c . At the same time the decrease of the irradiance level leads to a significantly weaker CLV and strong deviations from the measurements.

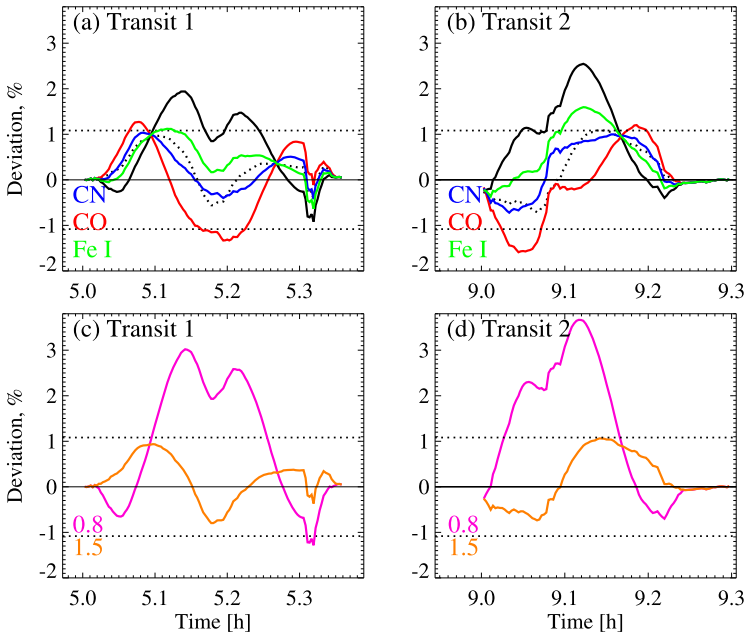


Figure 9 The deviations between the profiles as measured by unit 2 and as calculated with different modes of calculations with Model C. The “CN”, “CO”, and “Fe I” points were calculated scaling the additional opacity with the relative concentration of the corresponding species. The “0.8” and “1.5” points were calculated adjusting the additional opacity so that COSI yields 80 % and 150 % of the UV irradiance measured by SORCE/SOLSTICE. The black curve corresponds to the standard calculations using Model C. The dotted curve corresponds to the profile calculated with the empirical CLV.

Table 2 The discrepancies between the theoretical profiles calculated for different modes of calculations with Model C and for the altered levels of the SORCE/SOLSTICE measurements with observed and empirical profiles. The minimum values of the discrepancy for different modes of calculations with the Model C are boldfaced.

	Passage 1		Passage 2	
	Observed	Empirical	Observed	Empirical
Standard	105.0	90.9	129.3	111.5
CN	47.8	19.1	66.5	25.0
CO	83.4	73.3	85.4	60.8
Fe I	59.5	35.0	83.9	55.0
80 %	170.8	161.7	198.8	187.4
150 %	51.4	15.6	64.0	3.1

In Table 2 we compare profiles that were discussed above with the LYRA measurements. The first line corresponds to the calculations with height-independent additional opacity adjusted to reproduce the SORCE/SOLSTICE measurements. In Table 3 we list the coefficients from Equation (1) calculated with Models A, C, and E. The calculations with Model C are performed for three different cases of the additional opacity normalization. As discussed in Section 2, we employ a parabolic profile for the CLV, so only the first three coefficients from Equation (1) are different from zero. The exact theoretical CLV dependencies for all models and different wavelengths are available on request.

Table 3 Coefficients from Equation (1) calculated with different models of the solar atmosphere (Models C, A, and E). Calculations with Model C are performed for the case of height-independent additional opacity (“Standard”) and additional opacity scaled with the CN (“CN”), and Fe I (“Fe I”) relative concentrations.

	A_0	A_1	A_2
Empirical	0.1693	−0.0304	0.8611
Model C. Standard	0.1822	0.2122	0.6056
Model C. CN norm	0.1896	−0.1922	1.0026
Model C. Fe I norm	0.1859	−0.0190	0.8331
Model A	0.1056	0.1732	0.7212
Model E	0.2465	0.2350	0.5185

4. Conclusions

The profiles of the eclipse light curves provide important information for testing and refining solar atmospheric models. We have shown that the eclipse profiles observed by the Herzberg channel of LYRA are in a very good agreement with synthetic profiles calculated with the 1D NLTE radiative transfer code COSI.

The calculated profiles are very sensitive to the temperature structure of the solar atmosphere and to the treatment of the UV opacity, a significant part of which may still be missing from the modern models. The best agreement between the observed and measured profiles can be reached in two different regimes of calculations. The first corresponds to the calculations with the Model A atmosphere structure from Fontenla *et al.* (1999) and a constant coefficient of the additional opacity. The second is the calculation with Model C but assuming that the missing opacity scales with the relative concentration of neutral iron or CN molecule. Let us note that while the calculations with Model A are not able to properly reproduce the near UV, visible, and infrared solar irradiance, the calculations with Model C yield a good agreement with measurements over the entire solar spectrum (Shapiro *et al.*, 2010; Thuillier *et al.*, 2011).

Our results hint that the missing opacity originates in a layer a few hundred kilometers below the temperature minimum and could be due to unaccounted for lines of the neutral iron or another element with the similar ionization potential (*e.g.* silicon or magnesium) or due to the unaccounted for molecular lines (*e.g.* CN).

The nominal LYRA unit underwent substantial degradation before the next eclipse on 11 July 2010. The degradation affected the sensitivity of the unit and thus prevents us from repeating the analysis presented in Section 2.

The PREMOS instrument onboard the next European mission *Picard* (launched on 15 June 2010) measures the solar irradiance in five spectral passbands (two UV, one visible, and two infrared) and has already observed three solar eclipses (1 June, 1 July, and 25 November 2011). The analysis of the eclipses observed by PREMOS will be presented in a forthcoming article.

We are aware of the limitations of modeling with 1D solar atmosphere. Koesterke, Allende Prieto, and Lambert (2008) and Uitenbroek and Criscuoli (2011) show that 3D modeling can lead to a stronger CLV of the solar brightness. This prevents us from reaching an unambiguous conclusion. Nevertheless 1D radiative transfer codes are widely used for the interpretation of stellar and solar spectra and presently they are the *de-facto* standards for modeling the solar spectral-irradiance variability (Krivova and Solanki, 2008; Fontenla *et al.*, 2009; Domingo *et al.*, 2009).

The variability of the solar irradiance on 11-year and solar rotational time-scales is usually attributed to the competition between the irradiance increase due to the bright active components (*e.g.* plage and active network) and irradiance decrease due to dark sunspots

(Krivova *et al.*, 2003). The contrast between active features and the quiet Sun strongly depends on the disk position (Unruh, Solanki, and Fligge, 1999; Fligge, Solanki, and Unruh, 2000). Thus the center-to-limb variations of the solar brightness analyzed in this article play an important role in modeling of the solar-irradiance variability. The fact that the calculations with COSI are in good agreement with the measurements strongly supports its suitability for such modeling (Shapiro *et al.*, 2011d).

Acknowledgements The research leading to this article was supported by the Swiss National Science Foundation under grant CRSI122-130642 (FUPSOL) and grant 200020-130102. We thank the PROBA2/LYRA science team for their work in producing the data sets used in this article and their helpful recommendations. LYRA is a project of the Centre Spatial de Liège, the Physikalisch-Meteorologisches Observatorium Davos, and the Royal Observatory of Belgium funded by the Belgian Federal Science Policy Office (BELSPO) and by the Swiss Bundesamt für Bildung und Wissenschaft. PROBA2 is an ESA micro satellite operated by the Director for Science and Robotic Exploration.

References

- Allende Prieto, C., Asplund, M., Fabiani Bendicho, P.: 2004, Center-to-limb variation of solar line profiles as a test of NLTE line formation calculations. *Astron. Astrophys.* **423**, 1109–1117. doi:[10.1051/0004-6361/20047050](https://doi.org/10.1051/0004-6361/20047050).
- Benmoussa, A., Schühle, U., Haenen, K., Nesládek, M., Koizumi, S., Hochedez, J.-F.: 2004, PIN diamond detector development for LYRA, the solar VUV radiometer on board PROBA II. *Phys. Status Solidi, a Appl. Res.* **201**, 2536–2541. doi:[10.1002/pssa.200405187](https://doi.org/10.1002/pssa.200405187).
- Benmoussa, A., Dammasch, I.E., Hochedez, J.-F., Schühle, U., Koller, S., Stockman, Y., Scholze, F., Richter, M., Kroth, U., Laubis, C., Dominique, M., Kretzschmar, M., Mekaoui, S., Gissot, S., Theissen, A., Giordanengo, B., Bolsee, D., Hermans, C., Gillotay, D., Defise, J.-M., Schmutz, W.: 2009, Pre-flight calibration of LYRA, the solar VUV radiometer on board PROBA2. *Astron. Astrophys.* **508**, 1085–1094. doi:[10.1051/0004-6361/200913089](https://doi.org/10.1051/0004-6361/200913089).
- Berdugina, S.V., Solanki, S.K., Frutiger, C.: 2003, The molecular Zeeman effect and diagnostics of solar and stellar magnetic fields. II. Synthetic Stokes profiles in the Zeeman regime. *Astron. Astrophys.* **412**, 513. doi:[10.1051/0004-6361/20031473](https://doi.org/10.1051/0004-6361/20031473).
- Brasseur, G., de Rudder, A., Keating, G.M., Pitts, M.C.: 1987, Response of middle atmosphere to short-term solar ultraviolet variations. II. Theory. *J. Geophys. Res.* **92**, 903–914. doi:[10.1029/JD092iD01p00903](https://doi.org/10.1029/JD092iD01p00903).
- Busá, I., Andretta, V., Gomez, M.T., Terraneira, L.: 2001, A method to estimate the effect of line blanketing in NLTE radiative transfer calculations. *Astron. Astrophys.* **373**, 993–997. doi:[10.1051/0004-6361:20010661](https://doi.org/10.1051/0004-6361:20010661).
- Domingo, V., Ermolli, I., Fox, P., Fröhlich, C., Haberreiter, M., Krivova, N., Kopp, G., Schmutz, W., Solanki, S.K., Spruit, H.C., Unruh, Y., Vögler, A.: 2009, Solar surface magnetism and irradiance on time scales from days to the 11-year cycle. *Space Sci. Rev.* **145**, 337–380. doi:[10.1007/s11214-009-9562-1](https://doi.org/10.1007/s11214-009-9562-1).
- Dominique, M., Hochedez, J.-F., Schmutz, W., Dammasch, I., BenMoussa, A., Shapiro, A.I., Kretzschmar, M.: 2012, The LYRA instrument on-board PROBA2: description and in-flight performances. *Solar Phys.* submitted.
- Fligge, M., Solanki, S.K., Unruh, Y.C.: 2000, Modelling irradiance variations from the surface distribution of the solar magnetic field. *Astron. Astrophys.* **353**, 380–388. ADS: [2000A%26A...353..380F](https://ui.adsabs.org/2000A%26A...353..380F).
- Fontenla, J., White, O.R., Fox, P.A., Avrett, E.H., Kurucz, R.L.: 1999, Calculation of solar irradiances. I. Synthesis of the solar spectrum. *Astrophys. J.* **518**, 480–499. doi:[10.1086/307258](https://doi.org/10.1086/307258).
- Fontenla, J.M., Curdt, W., Haberreiter, M., Harder, J., Tian, H.: 2009, Semiempirical models of the solar atmosphere. III. Set of non-LTE models for far-ultraviolet/extreme-ultraviolet irradiance computation. *Astrophys. J.* **707**, 482–502. doi:[10.1088/0004-637X/707/1/482](https://doi.org/10.1088/0004-637X/707/1/482).
- Gray, D.F.: 1992, *The Observation and Analysis of Stellar Photospheres*, *Camb. Astrophys. Ser.* **20**, Cambridge Univ. Press, Cambridge. ADS: [1992oasp.book.....G](https://ui.adsabs.org/1992oasp.book.....G).
- Gray, L.J., Beer, J., Geller, M., Haigh, J.D., Lockwood, M., Matthes, K., Cubasch, U., Fleitmann, D., Harrison, G., Hood, L., Luterbacher, J., Meehl, G.A., Shindell, D., van Geel, B., White, W.: 2010, Solar influences on climate. *Rev. Geophys.* **48**, RG4001. doi:[10.1029/2009RG000282](https://doi.org/10.1029/2009RG000282).
- Haberreiter, M., Schmutz, W., Hubeny, I.: 2008, NLTE model calculations for the solar atmosphere with an iterative treatment of opacity distribution functions. *Astron. Astrophys.* **492**, 833–840. doi:[10.1051/0004-6361:200809503](https://doi.org/10.1051/0004-6361:200809503).

- Haigh, J.D.: 2007, The Sun and the Earth's climate. *Living Rev. Solar Phys.* **4**, 2. <http://www.livingreviews.org/lrsp-2007-2>. ADS: 2007LRSP...4....2H.
- Haigh, J.D., Winning, A.R., Toumi, R., Harder, J.W.: 2010, An influence of solar spectral variations on radiative forcing of climate. *Nature* **467**, 696–699. doi:10.1038/nature09426.
- Hamann, W.-R., Schmutz, W.: 1987, Computed He II spectra for Wolf–Rayet stars – A grid of models. *Astron. Astrophys.* **174**, 173–182. ADS: 1987A%26A...174..173H.
- Harder, J.W., Fontenla, J., Lawrence, G., Woods, T., Rottman, G.: 2005, The spectral irradiance monitor: measurement equations and calibration. *Solar Phys.* **230**, 169–204. doi:10.1007/s11207-005-1528-1.
- Harder, J.W., Fontenla, J.M., Pilewskie, P., Richard, E.C., Woods, T.N.: 2009, Trends in solar spectral irradiance variability in the visible and infrared. *Geophys. Res. Lett.* **36**, L07801. doi:10.1029/2008GL036797.
- Hestroffer, D., Mognan, C.: 1998, Wavelength dependency of the Solar limb darkening. *Astron. Astrophys.* **333**, 338–342. ADS: 1998A%26A...333..338H.
- Hochedez, J.-F., Schmutz, W., Stockman, Y., Schühle, U., Benmoussa, A., Koller, S., Haenen, K., Berghmans, D., Defise, J.-M., Halain, J.-P., Theissen, A., Delouille, V., Slemzin, V., Gillotay, D., Fussen, D., Dominique, M., Vanhellefont, F., McMullin, D., Kretzschmar, M., Mitrofanov, A., Nicula, B., Wauters, L., Roth, H., Rozanov, E., Rüedi, I., Wehrli, C., Soltani, A., Amano, H., van der Linden, R., Zhukov, A., Clette, F., Koizumi, S., Mortet, V., Remes, Z., Petersen, R., Nesládek, M., D'Olieslaeger, M., Roggen, J., Rochus, P.: 2006, LYRA, a solar UV radiometer on Proba2. *Adv. Space Res.* **37**, 303–312. doi:10.1016/j.asr.2005.10.041.
- Hubeny, I.: 1981, Non-LTE analysis of the ultraviolet spectrum of A type stars. II Theoretical considerations and interpretation of the VEGA Lyman-alpha region. *Astron. Astrophys.* **98**, 96–111. ADS: 1981A%26A....98...96H.
- Kishore Kumar, K., Subrahmanyam, K.V., John, S.R.: 2011, New insights into the stratospheric and mesosphere-lower thermospheric ozone response to the abrupt changes in solar forcing. *Ann. Geophys.* **29**, 1093–1099. doi:10.5194/angeo-29-1093-2011.
- Kleint, L., Shapiro, A.I., Berdyugina, S.V., Bianda, M.: 2011, Solar turbulent magnetic fields: Non-LTE modeling of the Hanle effect in the C2 molecule. *Astron. Astrophys.* **536**, 47. ADS: 2011A%26A...536A..47K.
- Koesterke, L., Allende Prieto, C., Lambert, D.L.: 2008, Center-to-limb variation of solar three-dimensional hydrodynamical simulations. *Astrophys. J.* **680**, 764–773. doi:10.1086/587471.
- Krivova, N.A., Solanki, S.K.: 2008, Models of solar irradiance variations: Current status. *J. Astrophys. Astron.* **29**, 151–158. doi:10.1007/s12036-008-0018-x.
- Krivova, N.A., Solanki, S.K., Unruh, Y.C.: 2011, Towards a long-term record of solar total and spectral irradiance. *J. Atmos. Solar-Terr. Phys.* **73**, 223–234. doi:10.1016/j.jastp.2009.11.013.
- Krivova, N.A., Solanki, S.K., Fligge, M., Unruh, Y.C.: 2003, Reconstruction of solar irradiance variations in cycle 23: Is solar surface magnetism the cause? *Astron. Astrophys.* **399**, 1–4. doi:10.1051/0004-6361:20030029.
- Kurucz, R.L.: 2005, Including all the lines. *Mem. Soc. Astron. Ital. Suppl.* **8**, 86. ADS: 2005MSAIS...8...86K.
- McClintock, W.E., Snow, M., Woods, T.N.: 2005, Solar-Stellar Irradiance Comparison Experiment II (SOLSTICE II): Pre-launch and on-orbit calibrations. *Solar Phys.* **230**, 259–294. doi:10.1007/s11207-005-1585-5.
- Neckel, H.: 1996, On the wavelength dependency of solar limb darkening ($\lambda\lambda 303$ to 1099 nm). *Solar Phys.* **167**, 9–23. ADS: 1996SoPh...167....9N, doi:10.1007/BF00146325.
- Neckel, H.: 2005, Analytical reference functions $F(\lambda)$ for the Sun's limb darkening and its absolute continuum intensities ($\lambda\lambda 300$ to 1100 m). *Solar Phys.* **229**, 13–33. doi:10.1007/s11207-005-4081-z.
- Neckel, H., Labs, D.: 1994, Solar limb darkening 1986–1990 ($\lambda\lambda 303$ to 1099 nm). *Solar Phys.* **153**, 91. ADS: 1994SoPh...153...91N, doi:10.1007/BF00712494.
- Rottman, G.: 2005, The SORCE mission. *Solar Phys.* **230**, 7–25. doi:10.1007/s11207-005-8112-6.
- Rozanov, E., Egorova, T., Schmutz, W., Peter, T.: 2006, Simulation of the stratospheric ozone and temperature response to the solar irradiance variability during Sun rotation cycle. *J. Atmos. Solar-Terr. Phys.* **68**, 2203–2213. doi:10.1016/j.jastp.2006.09.004.
- Schmutz, W., Hamann, W.-R., Wessolowski, U.: 1989, Spectral analysis of 30 Wolf–Rayet stars. *Astron. Astrophys.* **210**, 236–248. ADS: 1989A%26A...210..236S.
- Shapiro, A.I., Schmutz, W., Schoell, M., Haberreiter, M., Rozanov, E.: 2010, NLTE solar irradiance modeling with the COSI code. *Astron. Astrophys.* **517**, A48. doi:10.1051/0004-6361/200913987.
- Shapiro, A.I., Schmutz, W., Rozanov, E., Schoell, M., Haberreiter, M., Shapiro, A.V., Nyeki, S.: 2011a, A new approach to the long-term reconstruction of the solar irradiance leads to large historical solar forcing. *Astron. Astrophys.* **529**, A67. doi:10.1051/0004-6361/201016173.
- Shapiro, A.I., Fluri, D.M., Berdyugina, S.V., Bianda, M., Ramelli, R.: 2011b, NLTE modeling of Stokes vector center-to-limb variations in the CN violet system. *Astron. Astrophys.* **529**, A139. doi:10.1051/0004-6361/200811299.

- Shapiro, A.V., Rozanov, E., Egorova, T., Shapiro, A.I., Peter, T., Schmutz, W.: 2011c, Sensitivity of the Earth's middle atmosphere to short-term solar variability and its dependence on the choice of solar irradiance data set. *J. Atmos. Solar-Terr. Phys.* **73**, 348–355. doi:[10.1016/j.jastp.2010.02.011](https://doi.org/10.1016/j.jastp.2010.02.011).
- Shapiro, A.V., Shapiro, A.I., Schmutz, W., Dominique, M., Dammasch, I., Wehrli, C.: 2011d, Solar rotational cycle as observed by LYRA. *Solar Phys.* this issue.
- Shchukina, N., Trujillo Bueno, J.: 2001, The iron line formation problem in three-dimensional hydrodynamic models of solar-like photospheres. *Astrophys. J.* **550**, 970–990. doi:[10.1086/319789](https://doi.org/10.1086/319789).
- Short, C.I., Hauschildt, P.H.: 2005, A non-LTE line-blanketed model of a solar-type star. *Astrophys. J.* **618**, 926–938. doi:[10.1086/426128](https://doi.org/10.1086/426128).
- Short, C.I., Hauschildt, P.H.: 2009, Non-LTE modeling of the near-ultraviolet band of late-type stars. *Astrophys. J.* **691**, 1634–1647. doi:[10.1088/0004-637X/691/2/1634](https://doi.org/10.1088/0004-637X/691/2/1634).
- Sumod, S.G., Pant, T.K., Vineeth, C., Hossain, M.M., Antonita, M.: 2011, Response of the tropical mesopause to the longest annular solar eclipse of this millennium. *J. Geophys. Res.* **116**, A06317. doi:[10.1029/2010JA016326](https://doi.org/10.1029/2010JA016326).
- Thuillier, G., Floyd, L., Woods, T.N., Cebula, R., Hilsenrath, E., Hersé, M., Labs, D.: 2004, Solar irradiance reference spectra. In: Pap, J.M., Fox, P., Frohlich, C., Hudson, H.S., Kuhn, J., McCormack, J., North, G., Sprigg, W., Wu, S.T., (eds.) *Solar Variability and its Effects on Climate*, Washington Geophys. Monogr. Ser. **141**, 171. ADS: [2004GMS...141..171T](https://ui.adsabs.org/2004GMS...141..171T).
- Thuillier, G., Claudel, J., Djafer, D., Haberreiter, M., Mein, N., Melo, S.M.L., Schmutz, W., Shapiro, A., Short, C.I., Sofia, S.: 2011, The shape of the solar limb: Models and observations. *Solar Phys.* **268**, 125–149. doi:[10.1007/s11207-010-9664-7](https://doi.org/10.1007/s11207-010-9664-7).
- Uitenbroek, H., Criscuoli, S.: 2011, Why one-dimensional models fail in the diagnosis of average spectra from inhomogeneous stellar atmospheres. *Astrophys. J.* **736**, 69. doi:[10.1088/0004-637X/736/1/69](https://doi.org/10.1088/0004-637X/736/1/69).
- Unruh, Y.C., Solanki, S.K., Fligge, M.: 1999, The spectral dependence of facular contrast and solar irradiance variations. *Astron. Astrophys.* **345**, 635–642. ADS: [1999A%26A...345.635U](https://ui.adsabs.org/1999A%26A...345.635U).
- Vieira, L.E.A., Solanki, S.K., Krivova, N.A., Usoskin, I.: 2011, Evolution of the solar irradiance during the Holocene. *Astron. Astrophys.* **531**, A6. doi:[10.1051/0004-6361/201015843](https://doi.org/10.1051/0004-6361/201015843).